PERGAMON

International Journal of Solids and Structures 40 (2003) 1959–1972

INTERNATIONAL JOURNAL OF SOLIDS and STRUCTURES

www.elsevier.com/locate/ijsolstr

Evolution of penny-shaped microcracks by interface migration

Peizhen Huang [a,*], Jun Sun [a], Zhonghua Li [b]

[a] *State Key Laboratory for Mechanical Behaviour of Materials, School of Materials Science and Engineering, Xi'an Jiaotong University, 710049 Xi'an, PR China*

[b] *School of Civil Engineering and Mechanics, Shanghai Jiaotong University, 200240 Shanghai, PR China*

Received 28 March 2002; received in revised form 20 November 2002

Abstract

An axisymmetric finite element method is developed and employed to simulate healing evolution of intragranular penny-shaped microcracks under interface migration driven by total free energy change consisted of surface tension and chemical potential difference between phases. The validity of the method is confirmed by an agreement of the shrinkage and growth behavior, simulated numerically, of an isolated spherical grain with those predicted theoretically. The results showed that the surface tension alone serves to evolve the initial penny shape to a spherical one and, coupled with the chemical potential difference, dominates volume shrinkage of the microcracks. As the initial aspect ratio of a microcrack increases, both spheroidization and volume shrinkage times increase continuously. And the volume shrinkage process of the microcracks can be greatly promoted with an increase in the chemical potential difference.

Keywords: Penny-shaped microcrack; Interface migration; Shape change; Volume shrinkage; Axisymmetric finite element method

1. Introduction

When damage microcracks are generated in materials, the internal energy of the material increases together with some entropy increment, that is, the system is in a metastable state of the thermodynamic equilibrium. If some energy is imported from the environment, the system can overcome a potential barrier and automatically evolve along the way of minimizing the total Gibbs free energy (TGFE) of the system, so that the damage could be healed and the material performance could be partially restored. Otherwise, morphology of the damage microcracks, i.e. the sizes, shapes, volume fraction, and the mutual arrangement of the microcracks, plays an important role in determining mechanical, electric and magnetic properties of the material (Li and Chen, 1999). Therefore, it is essential to be able to understand microcrack evolution so that the microcrack healing mechanism can be comprehended and controlled to achieve a desired specific engineering requirement (Gao et al., 2000).

* Corresponding author.
E-mail address: pzhuang@mail.xjtu.edu.cn (P. Huang).

0020-7683/02/$ - see front matter
doi:10.1016/S0020-7683(03)00022-2

There have been many investigations into internal crack healing and similar morphological evolution processes over the past 40 years (Evans and Charles, 1977; Singh and Routbort, 1979; Drory and Glaeser, 1985; Scott and Tran, 1985; Carter and Glaeser, 1987; Rödel and Glaeser, 1988; Rödel and Glaeser, 1990a; Hsueh et al., 1982; Powers and Glaeser, 1993; Suo and Wang, 1994; Svoboda and Riedel, 1995). The microcrack shape changes under capillarity forces, namely chemical potential gradients arising from high surface curvature (Mullins, 1957; Bonzel, 1983; Drechsler, 1983). And in many practical situations microcrack evolution in polycrystalline materials occurs individually by solid state diffusion, the migration of interfaces, or a combination of these processes, depending on the sample profile (conical tip, grain boundary groove, simple or multiple scratches) and on experimental conditions (heating at low or high temperatures, vacuum annealing or heating in equilibrium vapor pressure, geometrical dimensions of the samples) (Binh and Uzan, 1987; Pan et al., 1997). It has been demonstrated, both theoretically and experimentally, that there are several geometrically distinct stages to the crack healing process in two dimensions (Rödel and Glaeser, 1990b; Powers and Glaeser, 1993; Huang et al., 2001, 2002). That is, significant progress has been made in modeling microcrack behavior controlled by solid state diffusion. And it can be said that the previous efforts have enabled us to relate many aspects of the macroscopic behavior of engineering materials to their microstructures and the underlying physical processes. The situation is, however, far from satisfactory, since real material systems are often complex and various, often unrealistic, assumptions have to be made in the material models in order to solve the mathematical equations (Pan et al., 1997). Especially, the kinetics of morphological evolution in axisymmetric microcracks (such as penny-shaped microcracks) has been given less-than-adequate attention. Only a few experimental studies have been reported (Evans and Charles, 1977; David and Evans, 1984; Yong and Wayne, 1987; Powers and Glaeser, 1992), most of which give only qualitative information. In comparison with a two-dimensional crack, an axisymmetric microcrack in three dimensions has two radii of curvature, the in-plane radius R_1 and the axisymmetric radius R_2, giving rise to more complex behaviors. The evolution of such cracks would be controlled by the driving forces induced by both curvatures. Therefore, there is a general lack of studies of three-dimensional morphological evolution of crack healing, despite of the obvious need to understand the phenomenon of crack healing in three dimensions. Until to now, to the author's knowledge, litter attention has been devoted to the healing evolution of penny-shaped microcracks by interface migration either on experimental investigations, or in numerical analyses. The aim of the present project reported here is mainly to numerically describe the morphological evolution of the penny-shaped microcracks by interface migration, and the relatively experimental works will be treated elsewhere.

Recently, a weak statement for surface motion has been formulated (Suo, 1997; Carter et al., 1997). It has weaker requirements on the smoothness of surface. On the basis of the weak statement, Sun et al. (1997) have developed a finite element program for simulation surface motion in two dimensions. Huang and Yang (1999) extended the two-dimensional finite element formulation to a three-dimensional (3D) finite element scheme to simulate the migration of interfaces in materials under linear kinetics. Kim and Kishi (1999) developed the method to simulate the Zener pinning behavior involving a three-dimensional effect without considering the chemical potential difference between the two adjacent phases in the TGFE of the system. The finite element method can capture intricate details in transient motion and readily includes multiple energetic forces and rate processes. Important physical conclusions were drawn from these numerical studies (Huang and Yang, 1999; Kim and Kishi, 1999; Kim et al., 1999; Kim, 2000, 2001; Prevost et al., 2001). However, the numerical technique has certain limitations, for instance, the axisymmetrical cases involving the chemical potential difference have not been reported in literature up to now.

In the present paper, an axisymmetric finite element formulation is developed to model the morphological evolution during the healing process of an intragranular microcrack controlled by the interface-migration kinetics as described in the classical paper of Mullins (1957), which also can be explored to simulate the morphology change of the second-phase precipitate particles. Considering the interface tension and the chemical potential difference between the two adjacent phases in the TGFE, we assume that surface

properties are independent of crystallographic orientations, namely surface energy and interface migration rate are isotropic. Thermodynamically, in the absence of applied stress, the morphology of a penny-shaped microcrack, similar to a single coherent particle, is determined by two factors: (1) the interfacial energy, and (2) the chemical potential difference between the matrix and the microcrack. And the interfacial energy of a microcrack is roughly proportional to its interfacial area, while the chemical potential difference is roughly proportional to its volume.

2. Axisymmetric finite element method

2.1. Weak statement of interface migration

When a solid particle is in contact with an environment (a vapor or a liquid solution), or an isolated precipitate surrounded by a matrix, the solid may gain mass from, or lose mass to, the environment, both causing the interface to move. The surface reaction is driven by the interfacial energy and by the chemical potential difference between the solid and the environment. In atomic scale, the movement of interface occurs by a thermally activated atomic jump across the interface. The driving force, p, for the atomic jump is supplied by a curvature-induced energy difference and the chemical potential difference per unit volume of atoms between the two adjacent phases Δg (i.e., the chemical potential of the solid minus that of the environment) (Suo, 1997).

$$p = -\kappa\gamma - \Delta g \tag{1}$$

where γ is the surface energy per unit area (or surface tension) and is assumed to be isotropic. The curvature of the interface κ is positive when the surface is concave. When $p = 0$, the solid is in equilibrium with the environment. When $p > 0$, the solid gains mass from the environment. When $p < 0$, the solid loses mass to the environment. As expected, γ tends to drive the solid surface in the direction toward the center of the curvature and Δg tends to cause the solid to shrink if $\Delta g > 0$.

The actual normal velocity of the interface motion, v_n, is a function of the driving force. For simplicity, we adopt a linear kinetic law (Sun et al., 1997; Prevost et al., 2001):

$$v_n = mp \tag{2}$$

Here m is the specific rate and depends on temperature in usual way, $m = m_0 \exp(-q/kT)$, where m_0 is the frequency factor, q is the activation energy, k is the Boltzmann's constant, and T is the temperature. The linear kinetic law (Eq. (2)) is a special case of a more general law introduced by Hilling and Charles (1965) and is valid when the driving force is small compared to the average thermal energy.

A virtual displacement, δr_n, of the interface is a motion in the direction normal to the interface and varies arbitrarily along the curved interface. It need not obey any kinetic law. Associated with the virtual motion, the total free energy of the system varies by an amount δG. Using the kinetic law (Eq. (2)), a weak statement of interface motion can be written as (Suo, 1997; Sun et al., 1997)

$$\int \frac{v_n \, \delta r_n}{m} \, \mathrm{d}A = -\delta G \tag{3}$$

The actual velocity distribution, v_n, satisfied Eq. (3) for arbitrary distributions of the virtual displacement.

2.2. An axisymmetric finite element

An axisymmetric surface is generated by rotating a plane curve around an axis lying on the same plane. In this paper, we introduce frustum elements to approach the surface of axisymmetric microstructure and

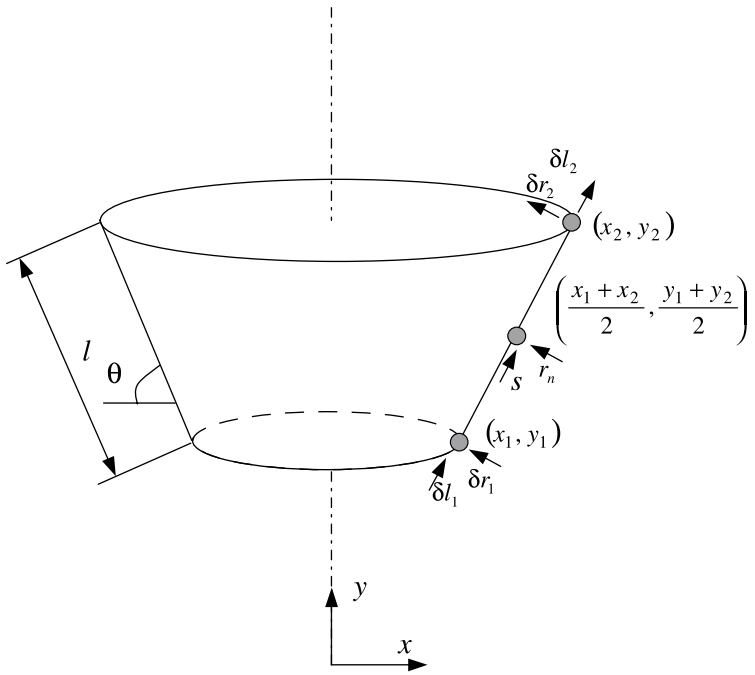

Fig. 1. A frustum element.

divide the generating curve into many small straight elements. The motions of the nodes describe the motion of the surface. Each node on the plane curve represents a circle on the surface in three dimensions. Fig. 1 shows one frustum element with two nodes (x_1, y_1) and (x_2, y_2) in two dimensions. The element has length l and slope θ, which relate to the coordinates of the two nodes as

$$x_2 - x_1 = h\cos\theta, \quad y_2 - y_1 = h\sin\theta \tag{4}$$

The local coordinate, s, is measured from the mid-point of the element. The surface area of the frustum element is $\pi(x_1 + x_2)l$, and the initial free energy, G_0^e, is

$$G_0^e = \gamma\pi(x_1 + x_2)l + \Delta g\,\Delta V \tag{5}$$

where ΔV is the volume of the frustum element.

For each surface element, the virtual motions of the nodes are

$$[\delta x_j]^e = [\,\delta x_1 \quad \delta y_1 \quad \delta x_2 \quad \delta y_2\,]_{\mathrm{T}} \tag{6}$$

Let $\dot{x}_1$, $\dot{y}_1$, $\dot{x}_2$ and $\dot{y}_2$ be the nodal velocities of the element. The generalized velocities are

$$[\dot{x}_j]^e = [\,\dot{x}_1 \quad \dot{y}_1 \quad \dot{x}_2 \quad \dot{y}_2\,]_{\mathrm{T}} \tag{7}$$

At a point, which has distance of s, its virtual displacement δr_n and normal velocity v_n have the relations as follows:

$$\begin{cases} \delta r_n = N_1\,\delta x_1 + N_2\,\delta y_1 + N_3\,\delta x_2 + N_4\,\delta y_2 \\ v_n = N_1\dot{x}_1 + N_2\dot{y}_1 + N_3\dot{x}_2 + N_4\dot{y}_2 \end{cases} \tag{8}$$

The interpolation coefficients are given by

$$\begin{cases} N_1 = -\left(\frac{1}{2} - \frac{s}{l}\right)\sin\theta & N_2 = \left(\frac{1}{2} - \frac{s}{l}\right)\cos\theta \\ N_3 = -\left(\frac{1}{2} + \frac{s}{l}\right)\sin\theta & N_4 = \left(\frac{1}{2} + \frac{s}{l}\right)\cos\theta \end{cases} \tag{9}$$

2.3. Nodal driving forces of the frustum element

For each element, the displacement of the node can be divided into two components. One, δl, is parallel to the element, and the other, δr, is normal to the element as shown in Fig. 1. When the two nodes move by Δl_1 and Δl_2, both the surface area and its volume of the axisymmetric element change, and the corresponding free energy varies by δG_l^e. Neglecting the terms of second order, δG_l^e can be represented as

$$\begin{aligned} \delta G_l^e = {} & 2\gamma\pi x_1\,\delta l_1 - 2\gamma\pi x_2\,\delta l_2 + \frac{\pi\Delta g}{3}\{(y_2 - y_1)\cos\theta[\delta l_1(2x_1 + x_2) + \delta l_2(2x_2 + x_1)] \\ & + (x_1^2 + x_2^2 + x_1x_2)(\delta l_2 - \delta l_1)\sin\theta\} \end{aligned} \tag{10}$$

The variation of the free energy caused by the displacement of the nodes in the normal direction (i.e., δr_1 and δr_2) is

$$\begin{aligned} \delta G_r^e = {} & \gamma\pi l\sin\theta\delta r_1 + \gamma\pi l\sin\theta\delta r_2 + \frac{\pi\Delta g}{3}\{-(y_2 - y_1)\sin\theta[\delta r_1(2x_1 + x_2) + \delta r_2(2x_2 + x_1)] \\ & + (x_1^2 + x_2^2 + x_1x_2)(\delta r_2 - \delta r_1)\cos\theta\} \end{aligned} \tag{11}$$

Then the total variation of the free energy can be expressed in terms of virtual motion of the nodes:

$$\delta G^e = -f_1\,\delta x_1 - f_2\,\delta y_1 - f_3\,\delta x_2 - f_4\,\delta y_2 \tag{12}$$

The force components acting on the two nodes due to the element surface tension and chemical potential difference Δg are

$$[f_i]^e = \gamma\pi\begin{bmatrix} 2x_1\cos\theta - l\sin^2\theta \\ 2x_1\sin\theta + l\sin\theta\cos\theta \\ -2x_2\cos\theta - l\sin^2\theta \\ -2x_2\sin\theta + l\sin\theta\cos\theta \end{bmatrix} + \frac{\pi\Delta g}{3}\begin{bmatrix} (2x_1 + x_2)(y_2 - y_1) \\ -(x_1^2 + x_2^2 + x_1x_2) \\ (2x_2 + x_1)(y_2 - y_1) \\ (x_1^2 + x_2^2 + x_1x_2) \end{bmatrix} \tag{13}$$

2.4. Viscosity matrix of the frustum element

Using Eqs. (8) and (9), and extending the integration over the surface of the frustum element, Eq. (3) becomes:

$$[\delta x_i]^{e^{\mathrm{T}}}[H_{ij}]^e[\dot{x}_j]^e = [\delta x_i]^{e^{\mathrm{T}}}[f_i]^e \tag{14}$$

where the viscosity matrix is

$$[H_{ij}]^e = \frac{\pi l}{6m}(x_1 + x_2)\begin{bmatrix} 2\sin^2\theta & -2\sin\theta\cos\theta & \sin^2\theta & -\sin\theta\cos\theta \\ -2\sin\theta\cos\theta & 2\cos^2\theta & -\sin\theta\cos\theta & \cos^2\theta \\ \sin^2\theta & -\sin\theta\cos\theta & 2\sin^2\theta & -2\sin\theta\cos\theta \\ -\sin\theta\cos\theta & \cos^2\theta & -2\sin\theta\cos\theta & 2\cos^2\theta \end{bmatrix} + \frac{\pi l^2\cos\theta}{6m}\begin{bmatrix} -\sin^2\theta & \sin\theta\cos\theta & 0 & 0 \\ \sin\theta\cos\theta & -\cos^2\theta & 0 & 0 \\ 0 & 0 & \sin^2\theta & -\sin\theta\cos\theta \\ 0 & 0 & -\sin\theta\cos\theta & \cos^2\theta \end{bmatrix} \tag{15}$$

The components of the viscosity matrix $[H_{ij}]^e$ and the force column $[f_i]^e$ depend on the nodal positions, and Eq. (14) is a set of non-linear ordinary differential equations. Since the equations are to hold for any variation $[\delta x_i]^{e^{\mathrm{T}}}$, we can obtain the controlling equation of the finite element

$$[H_{ij}]^e[\dot{x}_j]^e = [f_i]^e \tag{16}$$

The following procedure of the numerical simulation is the same as in two-dimensional problem (Sun et al., 1997; Kim and Kishi, 1999). We can calculate the velocity of all the discrete points on the curve (in two dimensions) by the above finite element method and let them advance by an amount $v_n\Delta t$ in a direction normal to the curve, where Δt is an appropriately chosen time increment. Repeat this procedure for many time steps to simulate the evolution of the microstructures.

3. Numerical simulations and discussion

It is known from Eq. (1) that the surface tension and the chemical potential difference of the two phases constitute a thermodynamic force, causing the microstructure, such as grains, microcracks and so on, to evolve. In this section, the grain growth and shrinkage are firstly simulated by the finite element method developed in this paper in order to check the reliability of the finite element method in simulating microstructure evolution. And the numerical results of the grain shrinkage driven by either surface tension alone or coupled with the chemical potential difference are compared with those theoretical predictions, respectively. Then, the finite element method is applied to analyze the healing evolution process of intragranular penny-shaped microcracks.

3.1. Grain growth and shrinkage

When a particle is heated, its shape evolves to reduce the free energy. Now we firstly consider an isolated spherical grain in an isotropic matrix with an identical chemical potential, and its growth behavior is caused only by surface tension. That is, the particle is in equilibrium with the environment and the driving force p is $-2\gamma/R$ in Eq. (1), where R is the radius of the spherical grain. In this case, the general kinetic law of grain growth is given by (Kim and Kishi, 1999)

$$\left(\frac{R}{R_0}\right)^n - 1 = K\,\widehat{t}_n \tag{17}$$

where R_0 is the initial radius and $\widehat{t}_n$, the normalized time ($= tm\gamma R_0^{-2}$). The value of K obtained by fitting a curve to Eq. (17) is -4.0 and $n = 2$, consistent with the theoretical values. The value of K for a two-dimensional case is -2.0 and $n = 2$. For $n = 2$ and $K = -4.0$, a driving force of $2\gamma/R$ is obtained for grain boundary movement by differentiating Eq. (17) with respect to time.

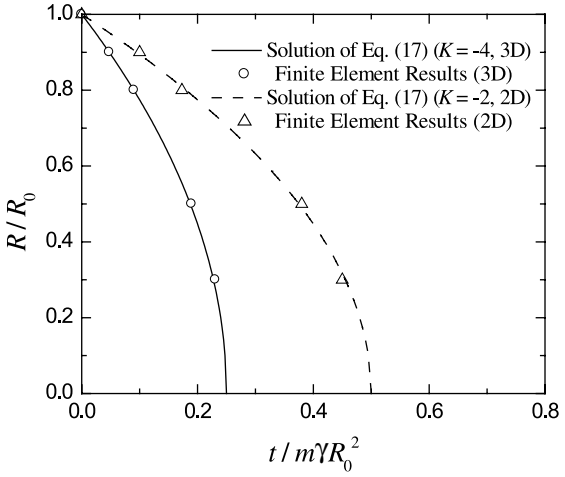

Fig. 2. Shrinkage behavior of the spherical grains.

The variation of the radius of the spherical grain R with respect to time obtained by finite element method is shown in Fig. 2, along with two-dimensional results. It is obvious that the numerical results agree well with the theoretical values.

Next consider a spherical particle immersed in a large mass of a vapor or solution. The system also has only one degree of freedom, R, the radius of the sphere. Within the environment, molecular mobility is so large that the chemical potential is taken to be uniform. The solid and the environment, however, are not in equilibrium with each other: the solid loses mass to the environment by dissolution. And the driving force on the surface of the spherical particle is $-(2\gamma/R) - \Delta g$. The total free energy can be written as

$$G = 4\pi R^2\gamma + \frac{4}{3}\pi R^3\,\Delta g \tag{18}$$

Here, γ is always positive, but Δg can be either positive or negative. For a positive Δg, the volume term reduces the free energy when the particle shrinks. In the case of $\Delta g < 0$, a critical radius R_c corresponding to maximal free energy is obtained by setting $\mathrm{d}G/\mathrm{d}R = 0$, giving

$$R_c = -2\frac{\gamma}{\Delta g} \tag{19}$$

Imagine a particle of radius $R \neq R_c$. Thermodynamics requires that the particle change size to reduce G. If $R > R_c$, the volume term in Eq. (18) becomes increasingly important, and the particle will expand to a larger and larger sphere to reduce G because $p > 0$. Contrarily, if $R < R_c$, the particle will shrink to a sphere and disappear.

From Eqs. (1) and (2), the analytical solution for the evolution of the spherical particle from an initial radius R_0 is given by (Suo, 1997)

$$(R - R_0) + R_c \ln\left|\frac{R - R_c}{R_0 - R_c}\right| = -m\,\Delta g t \tag{20}$$

The particle radius as a function of the time, $R(t)$, are shown by solid line in Fig. 3. The predictions based on the present FEM scheme are also plotted in Fig. 3 by dots. They agree very well with each other.

Hence, the present axisymmetric finite element formulation is valid in simulating the behavior of grain growth. And it is applicable for microstructure evolution not only controlled by surface tension, but also by both surface tension and the chemical potential difference between the two adjacent phases.

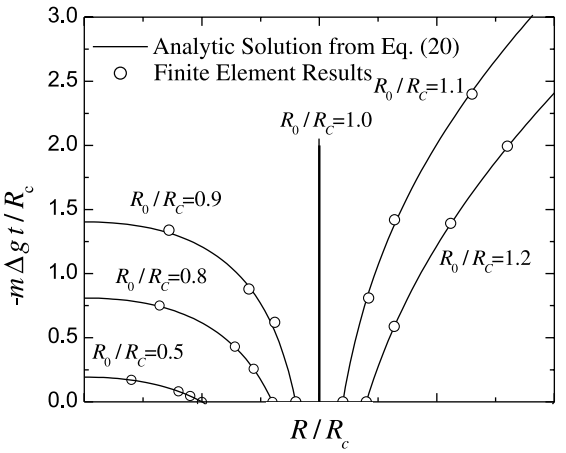

Fig. 3. Evolution of a spherical grain with isotropic surface tension and the chemical potential difference.

3.2. Evolution of intragranular penny-shaped microcracks

3.2.1. Microcrack evolution driven by isotropic surface tension alone

The free energy change to drive the interface migration has contributions from many origins. We now consider the evolution of an intragranular microcrack driven by the isotropic surface tension alone. In the present study, referring to the work of (Svoboda and Riedel, 1992), the accuracy of the numerical analysis was checked by comparing computations based on different node numbers with one another. We found that the differences between the model with different nodes are negligible when the total node number (N) is larger than 80. And for convenience, we introduce the dimensionless parameters: $\hat{t} = tm\gamma h_0^2$, $\Delta\hat{g} = \Delta g h_0/\gamma$, where the thickness of the microcrack h_0 is taken as 0.2 in all of the calculations. The initial shape of the intragranular microcrack is taken to be penny-shaped as shown in Fig. 4(a) at $\hat{t} = 0$, which is characterized by the aspect ratio β defined as the ratio of the diameter D_0 to the thickness h_0. The surface mobility m is assumed to be isotropic. At a fixed temperature, the intragranular microcrack evolves its shape because the curvature of the microcrack profile varies from point to point, which causes a migration of surface atoms from a point of higher curvature (higher chemical potential) to a point of lower curvature (lower chemical potential). Fig. 4 shows the simulation of an intragranular penny-shaped microcrack under the condition of $\beta = 10$. Since the microcrack evolution is only driven by the surface tension ($\Delta\hat{g} = 0$), that is, $R_c = \infty$, it is obvious that the volume of the microcrack will shrink as shown in Fig. 3. The microcrack simultaneously

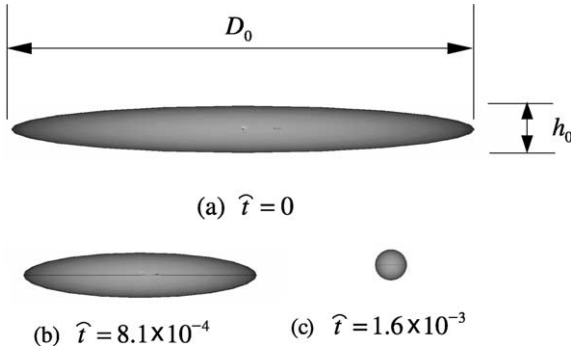

Fig. 4. The shape evolution of the penny-shaped microcrack of $\beta = 10$ driven by surface tension alone.

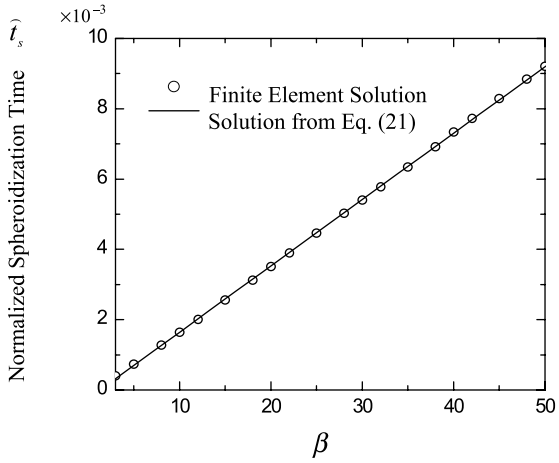

Fig. 5. The spheroidization time $\hat{t}_s$ of the penny-shaped microcracks only driven by surface tension as a function of β.

changes shape from a penny to a sphere and the mass in the grain leaves the grain, cross the microcrack surface, and join to the microcrack, leading to its shrinkage, as shown in Fig. 4 at $\hat{t} = 1.6 \times 10^{-3}$. This shape evolution process can be easily identified in many natural phenomena. Fig. 4 suggests that the microcrack always evolves to a spherical void eventually, independent from its initial shape.

By plotting the spheroidization time of the penny-shaped microcracks as a function of the original aspect ratio β (Fig. 5), we find that the spheroidization time increases roughly linearly in β because the transportation path of the mass is long for larger β. It can be best fitted using the following approximate formula:

$$\hat{t}_s = (-2.4932 + 1.889\beta) \times 10^{-4} \tag{21}$$

Fig. 6 shows the relative volume shrinkage V_s/V_0 as a function of time $\hat{t}$ for different values of β, where V_0 is the initial microcrack volume and V_s, the volume shrinkage. $V_s/V_0 = 1$ means that the microcrack completely vanishes, that is, the penny-shaped microcrack heals. As can be seen in Fig. 6, the microcrack healing time $\hat{t}_h$ consistently increases as β increases. The slope of these curves at any point represents the shrinkage rate of the microcrack volume. The curves in Fig. 6 show that, for a given penny-shaped

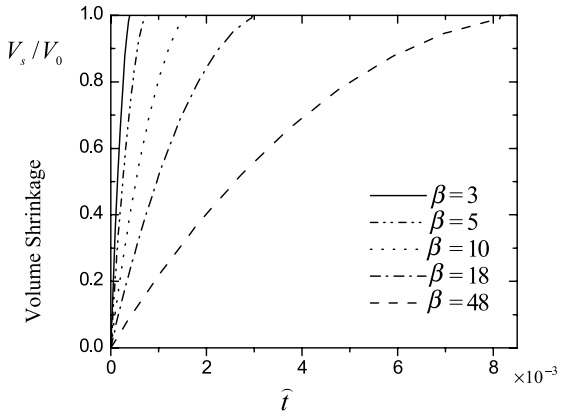

Fig. 6. Microcrack volume shrinkage—time behavior as a function of β.

microcrack, its volume shrinkage rate is greater at the beginning of the evolution process and then it becomes smaller gradually because the curvature variation along the microcrack surface is reduced continuously as its shape changes to a spherical one. And the curves also show that the volume shrinkage rate decreases with increasing β.

3.2.2. Microcrack evolution driven by surface tension and chemical potential difference

We next consider the case of the microcrack surface migration driven by interface tension and the chemical potential difference between the grain and the microcrack. Let us first examine the effect of the chemical potential difference $\Delta\hat{g}$ on the microcrack shape, which is shown in Fig. 7. For simplicity, the shapes are drawn in two dimensions, that is, Fig. 7 shows the cross section of the microcracks. When $\Delta\hat{g}$ is very small or even zero, the surface tension serves to change the initial penny shape to a spherical one.

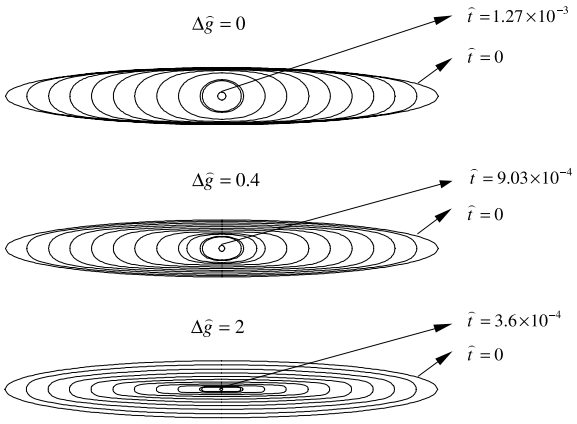

Fig. 7. A comparison of the microcrack shape for three values of $\Delta\widehat{g}$ for $\beta = 8$.

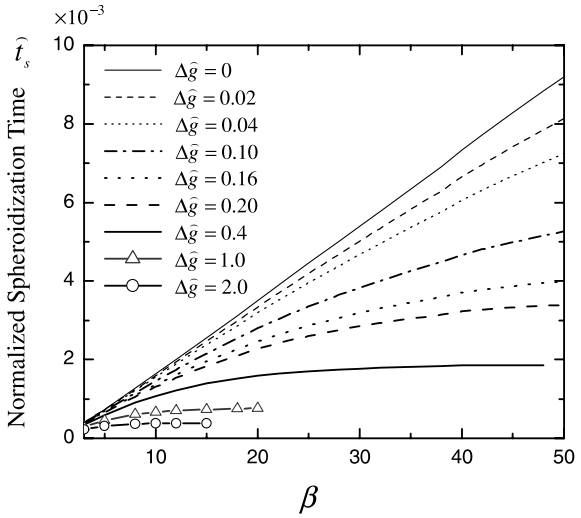

Fig. 8. The spheroidization time of the penny-shaped microcracks driven by surface tension and chemical potential difference as a function of β and $\Delta\widehat{g}$.

However, it is easy for the microcrack to evolve into a flat slit with increasing $\Delta\hat{g}$ (see the case of $\Delta\hat{g} = 2$ in Fig. 7) because the volume term gradually becomes dominant in Eq. (1).

Of course, the spheroidization time $\hat{t}_s$ does not only depend on the aspect ratio β but also on the chemical potential difference $\Delta\hat{g}$, as shown in Fig. 8. When $\Delta\hat{g} \leqslant 0.04$, $\hat{t}_s$ is a linear function of β for the given $\Delta\hat{g}$, that is, $\hat{t}_s$ is linearly proportional to β (similar to Eq. (21)) when the effect of the $\Delta\hat{g}$ is very small. But the relation between β and $\hat{t}_s$ becomes nonlinear gradually with increasing $\Delta\hat{g}$.

Fig. 9 shows the $\Delta\hat{g}$ dependence of the spheroidization time for three cases of β. The slope of these curves at any point represents the magnitude of the dependence. When $\beta = 10$, the $\Delta\hat{g}$ dependence of the spheroidization time is the greatest. Because the curvature along the microcrack surface is relatively smaller than the other two cases, the chemical potential difference becomes dominant in Eq. (1), that is, the surface tension is the weak driving force and the microcrack evolution mainly depend on $\Delta\hat{g}$. This is the reason why the effect of $\Delta\hat{g}$ on $\hat{t}_s$ is roughly linear when $\beta = 3$ as shown in Fig. 9.

Now, let us discuss the variation in the volume shrinkage rate with $\Delta\hat{g}$ and β. The volume shrinkage is shown in Fig. 10 as a function of time for various values of β in the case of $\Delta\hat{g} = 0.4$. Similar to the

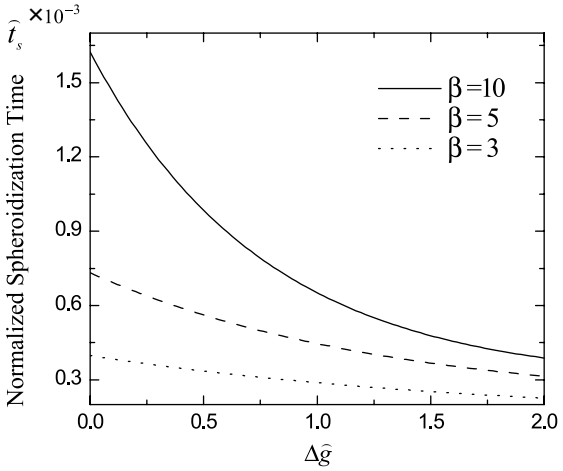

Fig. 9. The spheroidization time $\hat{t}_s$ of the penny-shaped microcracks for three values of β as a function of $\Delta\hat{g}$.

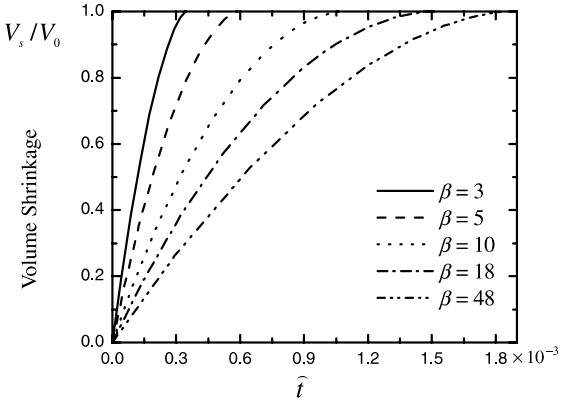

Fig. 10. Microcrack volume shrinkage—time behavior as a function of β for $\Delta\hat{g} = 0.4$.

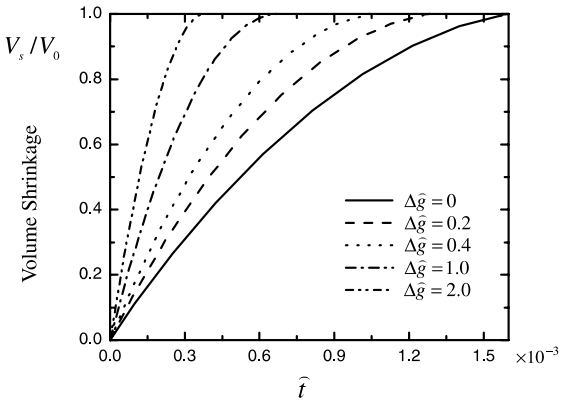

Fig. 11. Microcrack volume shrinkage—time behavior as a function of $\Delta\hat{g}$ for $\beta = 10$.

microcrack evolution driven by surface tension alone, the microcrack healing time $\hat{t}_h$ increases as β increases and the volume shrinkage is also faster at the beginning of the evolution process and then it becomes slower. Moreover, comparing with Fig. 6, we can find that the aspect ratio dependence of the volume shrinkage rate is relatively weakened with increasing $\Delta\hat{g}$ and it is obvious that, for the given β, the shrinkage rate is greater than that of the microcracks driven by surface tension alone. This means that the increase in $\Delta\hat{g}$ accelerates the shrinkage (or healing) rate of the penny-shaped microcracks.

Fig. 11 shows the $\Delta\hat{g}$ dependence of the shrinkage rate for $\beta = 10$ in detail. It is obvious that the healing time decreases with increasing $\Delta\hat{g}$, while the shrinkage rate increases continuously.

4. Concluding remarks

We formulated a finite element method for simulating the three-dimensional axisymmetric surface motion (or dissolution process) driven by surface tension and the chemical potential difference between the microstructure and the environment. The validity of the method was verified by comparing the results of the shrinkage behavior of an isolated spherical grain with the theoretical predictions.

The shape and volume evolutions of the intragranular penny-shaped microcracks were simulated during the microcrack healing processes. Our finite element results indicated that the spheroidization time and the rate of the microcrack volume shrinkage are related to the aspect ratio and the chemical potential difference between the intragranular microcrack and the surrounding matrix. When the effect of the chemical potential difference is very small ($\Delta\hat{g} \leqslant 0.04$), the spheroidization time increases roughly linearly in β. For the given penny-shaped microcrack, its volume shrinkage rate is greater at the beginning of the evolution process and then it becomes smaller gradually. And the volume shrinkage rate decreases with increasing β. When the aspect ratio is very small, the spheroidization time is a linear function of $\Delta\hat{g}$. The healing rate of the penny-shaped microcracks is accelerated by an increase in $\Delta\hat{g}$.

Acknowledgements

The financial support from the National Natural Science Foundation of China under grant no. 19972053 and 59889101 is gratefully acknowledged. One of the authors, Jun Sun, wishes to express his special thanks for the support of National Outstanding Young Investigator Grant of China through grant no. 59925104.

References

Binh, V.T., Uzan, R., 1987. Tip shape evolution: capillarity-induced matter transport by surface diffusion. I. Surf. Sci. 179, 540–560.

Bonzel, H.P., 1983. Mass transport by surface self-diffusion. In: Binh, V.T. (Ed.), Surface Mobilities on Solid Materials. In: NATO-ASI Series B-86. Plenum, New York, p. 195.

Carter, W.C., Glaeser, A.M., 1987. The morphological stability of continuous intergranular phases: thermodynamic considerations. Acta Metall. 35 (1), 237–245.

Carter, W.C., Taylor, J.E., Cahn, J.W., 1997. Variational methods for microstructural-evolution theories. JOM-J. Min. Met. Mat. S. 49 (12), 30–36.

David, L.S., Evans, B., 1984. Diffusional crack healing in quartz. J. Geophys. Res. 89, 4125–4135.

Drechsler, M., 1983. Mass transport by surface self-diffusion. In: Binh, V.T. (Ed.), Surface Mobilities on Solid Materials. In: NATO-ASI Series B-86. Plenum, New York, p. 191, 243.

Drory, M.D., Glaeser, A.M., 1985. The stability of pore channels: experimental observations. J. Am. Ceram. Soc. 68 (1), C-14–C-15.

Evans, A.G., Charles, E.A., 1977. Strength recovery by diffusive crack healing. Acta Metall. 25, 919–927.

Gao, Y.X., Fan, H., Xiao, Z., 2000. A simulation of asymmetrical voids evolution induced by electromigration. Mech. Mater. 32 (5), 315–326.

Hilling, W.B., Charles, R.J., 1965. Surface, stress-dependent surface reactions, and strength. In: Zackay, V.F. (Ed.), High Strength Materials. Wiley, New York, pp. 682–705.

Hsueh, C.H., Evans, A.G., Coble, R.L., 1982. Microstructure development during final/intermediate stage sintering. I. Pore/grain boundary separation. Acta Metall. 30, 1269–1279.

Huang, J.M., Yang, W., 1999. Three-dimensional evolution of interfaces under evaporation–condensation kinetics: a finite-element simulation. Model. Simul. Mater. Sci. Eng. 7, 87–105.

Huang, P.Z., Li, Z.H., Sun, J., 2001. The splitting and cylinderization processes of damage microcracks analyzed by finite element method. Model. Simul. Mater. Sci. Eng. 9 (3), 193–206.

Huang, P.Z., Li, Z.H., Sun, J., 2002. The shrinkage and splitting processes of damage microcracks under pressure simulated by finite element method. Metall. Mater. Trans. A 33, 1117–1124.

Kim, B.N., Kishi, T., 1999. Finite element simulation of Zener pinning behavior. Acta Mater. 47 (7), 2293–2301.

Kim, B.N., Hiraga, K., Sakka, Y., Ahn, B.W., 1999. A grain-boundary diffusion model of dynamic grain growth during superplastic deformation. Acta Mater. 47 (12), 3433–3439.

Kim, B.N., 2000. Analyses of grain growth behavior in particle-dispersed materials by finite element simulation. J. Jpn. I. Met. 64 (1), 21–26, in Japanese.

Kim, B.N., 2001. Modeling grain growth behavior inhibited by dispersed particles. Acta Mater. 49 (3), 543–552.

Li, D.Y., Chen, L.Q., 1999. Shape evolution and splitting of coherent particles under applied stresses. Acta Mater. 47 (1), 247–257.

Mullins, W.W., 1957. Theory of thermal grooving. J. Appl. Phys. 28 (3), 333–339.

Pan, J., Cocks, A.C.F., Kucherenko, S., 1997. Finite element formulation of coupled grain-boundary and surface diffusion with grain-boundary migration. Proc. R. Soc. Lond. A 453, 2161–2184.

Powers, J.D., Glaeser, A.M., 1992. Higher-temperature healing of cracklike flaws in Mg- and Ca-ion-implanted sapphire. J. Am. Ceram. Soc. 75 (9), 2547–2558.

Powers, J.D., Glaeser, A.M., 1993. Higher-temperature healing of cracklike flaws in Titanium ion-implanted sapphire. J. Am. Ceram. Soc. 75 (9), 2225–2234.

Prevost, J.H., Baker, T.J., Liang, J., Suo, Z., 2001. A finite element method for stress-assisted surface reaction and delayed fracture. Int. J. Solids Struct. 38, 5185–5203.

Rödel, J., Glaeser, A.M., 1988. In: Yoo, M.H., Clark, W.A.T., Braint, C.L. (Eds.), Interfacial Structures Properties and Design. Materials Research Society, Pittsburgh, PA, pp. 485–490.

Rödel, J., Glaeser, A.M., 1990a. In: Handwerker, C., Blendell, J.E., Kaysser, W.A. (Eds.), Sintering of Advanced Ceramics. The American Ceramic Society, B. Westerville, OH, pp. 243–257.

Rödel, J., Glaeser, A.M., 1990b. High-temperature healing of lithographically introduced cracks in sapphire. J. Am. Ceram. Soc. 73 (3), 592–601.

Scott, C., Tran, V.B., 1985. Diffusion bonding of ceramics. Am. Ceram. Soc. Bull. 64 (8), 1129–1131.

Singh, R.N., Routbort, J.L., 1979. Fracture and crack healing in (U, Pu) C. J. Am. Ceram. Soc. 62 (3-4), 128–133.

Suo, Z., Wang, W., 1994. Diffusive void bifurcation in stressed solid. J. Appl. Phys. 76 (6), 3410–3421.

Suo, Z., 1997. Motions of microscopic surfaces in materials. Adv. Appl. Mech. 33, 193–294.

Sun, B., Suo, Z., Yang, W., 1997. A finite element method for simulating interface motion. I. Migration of phase and grain boundaries. Acta Mater. 45 (5), 1907–1915.

Svoboda, J., Riedel, H., 1992. Pore-boundary interactions and evolution equations for the porosity and the grain size during sintering. Acta Mater. 40 (11), 2829–2840.

Svoboda, J., Riedel, H., 1995. Quasi-equilibrium sintering for coupled grain-boundary and surface diffusion. Acta Metall. Mater. 43 (2), 499–506.

Yong, L.T., Wayne, K.R., 1987. Mechanisms of pearlite spheroidization. Metall. Trans. 18A, 1403–1414.